Archives of Acoustics Vol. 51, No. 1, pp. 183–196 (2026), https://doi.org/10.24423/archacoust.2026.4286

Technical Note

Similarity Analysis and Target Strength Correction of Non-Proportional Scaled Models Based on Highlight Model Theory

Jin Zhang[(1),(2)], Zhenyu Li[(3)], Yinhao Li[(3)], Zilong Peng[(3)*]

[(1)] *Beijing Institute of Technology*
Beijing, China

[(2)] *Jiangsu Automation Research Institute*
Lianyungang, China

[(3)] *School of Energy and Power, Jiangsu University of Science and Technology*
Zhenjiang, China

*Corresponding Author: zlp_just@sina.com

Received July 23, 2025; revised December 30, 2025; accepted December 30, 2025; version of record March 18, 2026; published issue March 27, 2026.

Acoustic scattering scale models often fail to meet the acoustic similarity design requirements due to limitations in fabrication technology, testing facilities, and safe transportation, which restrict the accurate extrapolation of acoustic scattering characteristics between scaled models and full-scale ships. To overcome this challenge, the present study applies highlight model theory to perform acoustic similarity analysis and to correct the local target strength of simple objects in the model based on overall acoustic scattering correction. A novel method for correcting the target strength of non-proportional scaled models is proposed. The method is validated using various model geometries, including ellipsoids, finite-length cylinders, truncated elliptical cones, and complex structures. Additionally, the plate element method is employed for target strength correction and scaling conversion analysis for non-proportional scaled models. The study highlights the variation in target strength due to changes in geometric dimensions and demonstrates the effectiveness of the proposed correction method. The results indicate that the proposed correction approach allows for more accurate extrapolation of target strength from non-proportional scaled models to full-scale prototypes, thereby better satisfying the requirements of practical engineering applications.

Keywords: acoustic scattering, similarity theory, highlight theory, scaled model.

1. Introduction

Underwater target acoustic scattering experiments are categorized into full-scale ship tests and scaled model tests. Scaled model tests involve conducting experiments using a scaled-down model under controlled conditions (Tang *et al.*, 2018). These tests offer enhanced controllability and repeatability, making them ideal for in-depth analysis of scattering mechanism. Gao and Lin (2019) performed pool tests on a novel underwater vehicle, designing and validating a system capable of five degrees of freedom movement, thus confirming the feasibility of using fan-shaped wings underwater. Ke *et al.* (2024) investigated the acoustic scattering characteristics of a propeller through lake tests, validating a static acoustic scattering prediction method for ship propellers with complex linear geometries. Liu *et al.* (2023) conducted acoustic scattering tests on a 1/16 scaled model of an underwater vehicle, validating the accuracy of a patch-correction highlight model prediction approach. Xue *et al.* (2023) performed acoustic target strength tests on a benchmark scaled model, verifying the reliability of

the curved element method through comparison with the plate element method. Zhou *et al.* (2021) designed a ship shafting propulsion system using aerodynamic scaling relations, confirming the design's feasibility through simulations and experiments. Yu *et al.* (1999; 2002a) carried out similarity tests on structural vibrations in air and sound radiation in water for a ribbed cylindrical shell model, establishing corresponding similarity scaling relationships.

Scaled model multi-base elastic wave tests enable the analysis of elastic wave generation mechanisms and propagation paths (Agounad *et al.*, 2020; 2023; Ting *et al.*, 2019). Stulenkov *et al.* (2024) examined the acoustic field of a propeller, focusing on the resonance frequencies of its blades, using a combination of numerical simulations and experimental physical modeling. They also demonstrated the influence of the Q-factor on the radiation spectrum through propeller models made from different materials. Yan and Wang (2025) developed a composite structure model using thin-film metamaterials for low-frequency underwater sound absorption. The model was fabricated and validated through numerical simulations and experiments, and the effects of material properties, thickness, and mass block distribution on acoustic performance were analyzed, providing new insights for underwater stealth technology. Tao *et al.* (2025) proposed a deep learning model based on low-frequency analysis and recording (LOFAR) spectral features to mitigate the impact of ship underwater radiated noise (VURN) on underwater acoustic communication. Simulations and experiments demonstrated that the proposed method offers greater robustness and lower bit error rates under varying signal-to-noise ratios. Feng *et al.* (2025) introduced a time-difference-of-arrival (TDOA) sequence estimation method based on a hidden Markov model (HMM) for passive positioning systems with wideband underwater moving sound sources and distributed hydrophones. The effectiveness of the method was validated through simulations and lake experiments. Although these studies differ in their research objectives and methodologies, they all employ scale model experiments to empirically validate theoretical analyses, numerical simulations, or design concepts under controlled conditions. However, they focus exclusively on geometrically scaled models rather than non-geometrically scaled models.

Non-proportional scaled models can lead to inaccurate conclusions or data deviations, undermining the credibility and scientific value of research. To mitigate the impact of non-proportional scaling on experiments, large-scale models are often employed to simplify model fabrication. For example, the United States developed the large-scale 'Kamloops' model for sonar fairing design, while the large scale vehicle (LSV) series models were also used for testing to enhance design (Liu *et al.*, 2017). Wang *et al.* (2024) proposed a novel similarity method for box girders subjected to combined effects of bending moments and lateral pressure, which disregards the similarity criteria of cross-sectional properties and instead focuses solely on strength-based similarity criteria. Using this approach, similarity relations for the ultimate moment and applied lateral pressure were derived, and a step-by-step procedure for scale model design was proposed. Ge *et al.* (2024) introduced a discretized macro-element (DME) method that integrates experimental, numerical, and analytical techniques to rapidly assess the crushing behavior and protective performance of crashworthy devices in ship collisions. Based on similarity laws, the crush curve for large crashworthy devices was derived, and the advantages of the DME method in accurately capturing local deformation and improving computational efficiency were demonstrated. Liu *et al.* (2024) conducted wave pool experiments to investigate the hydrodynamic response characteristics of a scaled model of a submerged floating tunnel (SFT) and the effects of local cable breakage. The results indicated that under lower wave excitation, self-vibration of the SFT becomes more pronounced, and the response is more sensitive to variations in cable force, which is also influenced by immersion depth. Li *et al.* (2020) developed a method to assess the structural performance of beams on ultra-large container ships. A scaled model testing system based on Buckingham's theorem and Froude scaling law was implemented, and systematic experimental and numerical analyses were conducted on the stay cables, providing substantial support for the design and optimization of ultra-large cable-stayed bridges. To address potential biases introduced by non-proportional scaled models, current research is shifting from traditional geometric similarity toward a deeper focus on physical mechanism similarity, with an emphasis on developing tailored similitude criteria for specific structural responses.

Yu and Lu (2001) and Yu *et al.* (2002b) employed the energy method to analyze the loss factor, surface sound reflection, and scale effects caused by small mass blocks in large-scale acoustic models of underwater vehicles, controlling these effects through model design. However, the fabrication of large-scale models is costly, requires

specialized experimental equipment, and imposes high demands on the width and depth of the test water area. During the construction of scaled models, material losses inevitably affect acoustic similarity. To address the limitations of traditional proportional scaling schemes in meeting rigid-body overload similarity requirements, Liu *et al.* (2020) investigated non-proportional scaling penetration similarity laws and proposed a corresponding non-proportional scaling test design method. Wang *et al.* (2021) focused on material properties and introduced dimensionless numbers to characterize the similarity of strain hardening, strain-rate sensitivity, and temperature softening effects, based on similarity analysis of the thermal-viscosity constitutive equation. Wang *et al.* (2023) examined the scaling characteristics of geometrically distorted models using similarity criteria and design methods, analyzing various combinations of scaled models and providing guidance on the design of scaled models. Zhang *et al.* (2001) applied similarity theory to analyze key dimensionless quantities in the cylindrical shell sound field formula and employed material compensation to maintain similarity between the compensated sound field and the prototype sound field. By effectively correcting the data, the accuracy of scaled-model results can be enhanced. Huijgens *et al.* (2021) accurately simulated the interaction between the propeller and the engine by correcting viscous scale effects and torsional axis dynamics through testing.

From the early focus on performance control of large-scale acoustic models, to the establishment of scaling laws with non-geometric similarity for mechanical processes, and further to in-depth similarity analysis and compensation of material constitutive properties and geometric characteristics, research has progressively advanced in scaled-model studies. The correction methods for scaled models outlined above primarily focus on the models themselves. These methods involve utilizing large-scale models, adjusting the physical properties of materials, and correcting influencing parameters, with the aim of minimizing the potential impact of geometric scaling on scaled-model experiments. However, the effects of non-proportional scaling on target strength, as well as methods for correcting target strength in non-proportional scaled models, remain areas requiring further investigation. The concept of non-proportional scaling is illustrated in Fig. 1. To address these challenges, this study proposes a correction approach based on highlight model theory (Tang *et al.*, 1994), integrated with sound-scattering similarity, to effectively correct the results of scaled-model experiments and enhance their accuracy and reliability. The findings demonstrate that this correction method is not only theoretically sound but also holds significant practical application value in real-world experiments.

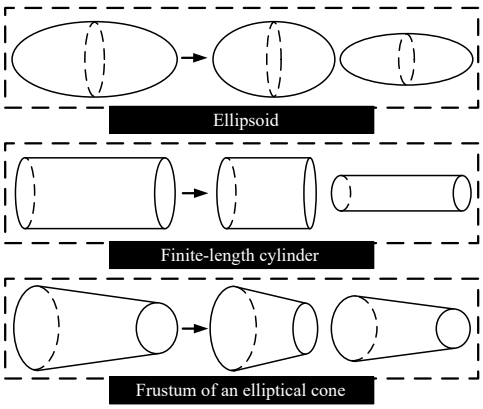

Fig. 1. Diagram of the non-proportional scaling of the base model.

The work presented in this paper is structured as follows. First, correction methods for the target strength of scaled models under various operating conditions (ellipsoid, finite-length cylinder, and frustum) are derived using highlight model theory. Second, the plate element method (Fan *et al.*, 2012) is employed to correct the target strength of the scaled models under different operating conditions, with the corrected results compared to the target strength of the prototype to assess the feasibility of the correction method. Finally, a complex computational model is developed to further correct the target strength of the scaled model. By comparing the corrected results with those of the prototype, the applicability and effectiveness of the proposed correction method are validated.

2. Geometric highlight model of simple targets

The primary theoretical modeling methods for underwater target echo characteristics can be categorized into two approaches: the 'decomposition-synthesis' method (also known as the component method) and the numerical integration method. In the component method, the echo of each individual component or sub-target is modeled using a highlight model derived from physical acoustics. This model, referred to as the 'highlight model,' is particularly suitable for engineering applications. This paper provides a comprehensive overview of the shape features of underwater vehicles and derives the geometric highlight parameters for several typical sub-targets, as illustrated in Fig. 2.

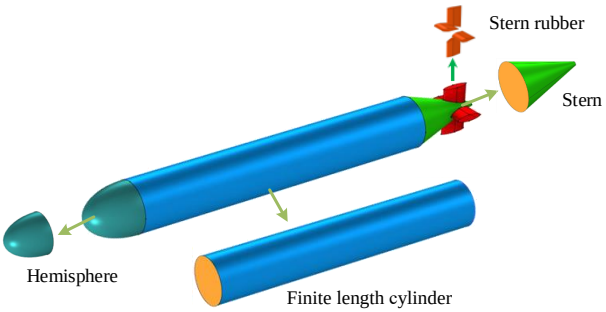

Fig. 2. 3D model of an underwater vehicle and its component decomposition.

The underwater vehicle is composed of simple geometric components, including an ellipsoid at the bow, a cylindrical section at the mid-body, and an elliptical-cone frustum at the stern, along with the sail housing, elevators, and stern rudders (Schneider *et al.*, 2003). In Fig. 2, when assembling the vehicle from components such as the hemisphere, finite-length cylinder, and sail housing, the spatial position relationships between the components are not taken into account. Instead, an incoherent superposition method is employed.

The method proposed in this paper is based on the 'highlight model' theory. The highlight model is an approximate method applicable under high-frequency conditions, and this study primarily focuses on the geometric components of underwater vehicles. These vehicles are mostly rigid structures, and the study mainly concerns structures made of structural steel.

During underwater scaled-model testing, factors such as manufacturing tolerances and transportation constraints may prevent the target strength of the scaled model from being directly converted to that of the prototype using scaling ratios. The method proposed in this paper can be applied to correct the target strength of the scaled model. The geometric highlight model for simple targets is primarily used to calculate unscaled structures. In practical applications, it can be utilized to correct the acoustic target strength of imperfectly scaled models, thereby establishing a link between the acoustic target strength of the scaled model and that of the prototype.

2.1. Ellipsoid

The ellipsoid is a fundamental geometric shape commonly used as an approximation in early echo prediction models for underwater vehicles. It is also one of the first types of sub-targets to be studied. When the major and minor axes are equal, the ellipsoid degenerates into a sphere. This shape can effectively approximate the head of an underwater vehicle.

The coordinate system is shown in Fig. 3, where the ellipsoid's semi-major axis is denoted as a and the semi-minor axis as b. When a sound wave is incident at an angle of φ, the highlight transfer function of the rotating ellipsoid can be derived using physical acoustics methods and the stationary-phase integration:

$$H(\mathbf{r}\omega) = \frac{1}{2}\frac{a^2\sin^2 v_0 + b^2\cos^2 v_0}{a} e^{2i\omega\sqrt{(b\sin v_0)^2+(a\cos v_0)^2}\cos(\varphi-a)/c}, \tag{1}$$

where $\tan v_0 = (b/a)\tan\varphi$, $\tan\alpha = (b/a)^2\tan\varphi$, and c is the sound speed in water, ω is the angular frequency. When the semi-major and semi-minor axes are equal, (i.e., $a = b$), the transfer function for a spherical target

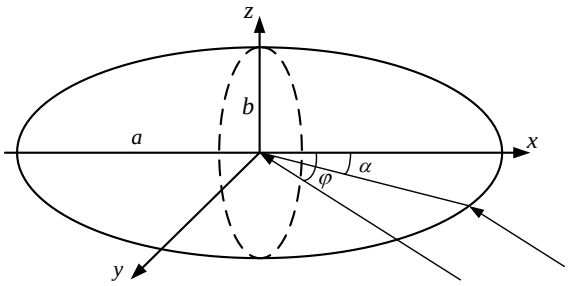

Fig. 3. Diagram for calculating the echo of an ellipsoid.

is obtained. In the transfer function, the phase factor represents the transmission path of the echo. Ignoring the phase factor, the target strength formula for the ellipsoid is expressed as

$$\mathrm{TS} = 20\log(H(\mathbf{r}\omega)) = 20\log\left(\frac{1}{2}\frac{a^2\sin^2 v_0 + b^2\cos^2 v_0}{a}\right). \tag{2}$$

2.2. Finite-length elliptical cylinder

The finite-length elliptical cylinder is a significant type of sub-target. The shapes of early submarine sail enclosures, tail fins, and diving planes closely resemble an elliptical cylinder. When the major and minor axes are equal, the elliptical cylinder degenerates into a cylindrical shape. This model can be used to approximate both the pressure hull and non-pressure hull sections of a submarine. A finite-length cylindrical shape is illustrated in Fig. 4. In this configuration, the long semi-axis (a) of the ellipse aligns with the x-axis, the short semi-axis (b) is along the y-axis, and the side length (h) is oriented along the z-axis. This discussion focuses on the case of vertical incidence with respect to the z-axis, where the sound wave propagates in the xy-plane. Under these conditions, only the echo from the side needs to be considered. The target strength of the finite-length elliptical cylinder is given by

$$\mathrm{TS} = 10\log\left(\frac{1}{\lambda^2}|I|^2\right). \tag{3}$$

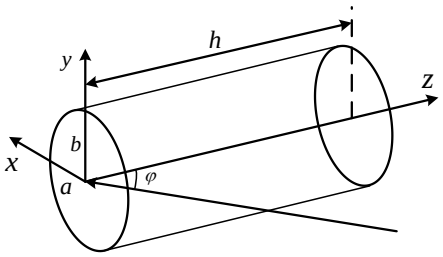

Fig. 4. Diagram for calculating the echo of a finite-length elliptical cylinder.

The phase factor represents the propagation path of the echo. After neglecting the phase factor, the expression for I becomes:

$$I = \sqrt{\frac{\pi}{k}}\frac{hab}{(a^2\cos^2\varphi + b^2\sin^2\varphi)^{3/4}}, \tag{4}$$

where k denotes the wave number ($k = \pi/\lambda$), h represents the height of the finite-length elliptical cylinder, a and b correspond to the long and short semi-axes of the elliptical cylinder, respectively, and λ is the wavelength.

2.3. Frustum of an elliptical cone

A frustum of an elliptical cone is a significant type of sub-target, from which a frustum of a circular cone can be derived. Both the front and rear edges of the frustum have a specific slope, and it can be utilized to approximate control surfaces such as the fuselage rudder, horizontal tailplane, and vertical tailplane, either individually or in combination with other basic geometric shapes. The frustum of an elliptical cone is illustrated in Fig. 5.

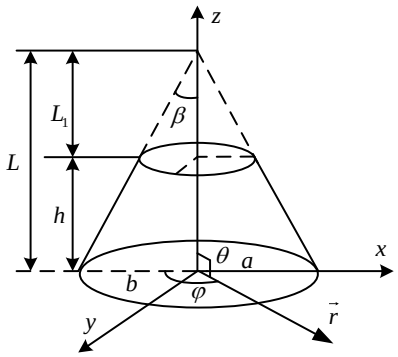

Fig. 5. Diagram for calculating the echo of a frustum of an elliptical cone.

The key parameters of the elliptical cone frustum include the semi-major axis (a) and semi-minor axis (b) of the upper base, the height (L) of the upper section, the height of the lower base (L_1) and the half-apex angle (β). The highlight on the frustum of the elliptical cone can also be equivalently regarded as the edge points of the upper and lower edges. By applying methods from physical acoustics and stationary-phase analysis, the following expression for the highlight transfer function can be derived:

$$H(\mathbf{r}\omega) = H_1(\mathbf{r}\omega) + H_2(\mathbf{r}\omega), \tag{5}$$

$$H_1(\mathbf{r}\omega) = A_1 e^{i\omega\tau_1} e^{i\varphi_1}, \tag{6}$$

$$H_2(\mathbf{r}\omega) = A_2 e^{i\omega\tau_2} e^{i\varphi_2}, \tag{7}$$

$$A_1 = \frac{1}{4}\sqrt{\frac{L}{\pi k}} \frac{\eta^{3/2}\tan^{1/2}\beta}{\sin^{1/2}\theta(\sin^2\varphi+\eta^2\cos^2\varphi)^{1/4}} \frac{\sin\theta(\sin^2\varphi+\eta^2\cos^2\varphi)^{-1/2} - \frac{1}{\eta}\tan\beta\cos\theta}{\sin\theta\tan\beta(\sin^2\varphi+\eta^2\cos^2\varphi)^{1/2}+\eta\cos\theta}, \tag{8}$$

$$A_2 = \frac{1}{4}\sqrt{\frac{L_1}{\pi k}} \frac{\eta^{3/2}\tan^{1/2}\beta}{\sin^{1/2}\theta(\sin^2\varphi+\eta^2\cos^2\varphi)^{1/4}} \frac{\sin\theta(\sin^2\varphi+\eta^2\cos^2\varphi)^{-1/2} - \frac{1}{\eta}\tan\beta\cos\theta}{\sin\theta\tan\beta(\sin^2\varphi+\eta^2\cos^2\varphi)^{1/2}+\eta\cos\theta}, \tag{9}$$

$$\tau_1 = 2L\left(\sin\theta\tan\beta\left(\cos^2\varphi+\frac{1}{\eta^2}\sin^2\varphi\right)^{1/2}+\cos\theta\right)\Big/c, \tag{10}$$

$$\tau_2 = 2L_1\left(\sin\theta\tan\beta\left(\cos^2\varphi+\frac{1}{\eta^2}\sin^2\varphi\right)^{1/2}+\cos\theta\right)\Big/c, \tag{11}$$

where $\varphi_1 = -\frac{5}{4}\pi$, $\varphi_2 = -\frac{1}{4}\pi$, $\eta = \frac{a}{b}$.

The phase factor represents the propagation path of the echo. By neglecting the phase factor, the target strength of the frustum of an elliptical cone is given by

$$\mathrm{TS} = 20\log(H(\vec{r}\omega)) = 20\log(A_1 + A_2). \tag{12}$$

3. Target strength correction for scale models

This section focuses on ellipsoids, finite-length elliptical cylinders, and frustums of elliptical cones as the primary research objects. By combining acoustic similarity theory with the geometric scattering model theory, a correction method for the target strength of non-geometrically scaled models is developed. The proposed correction method is subsequently validated using the plate element method.

3.1. Correction of target strength for the ellipsoid

The target strength formula for the ellipsoid, derived in Subsec. 2.1, demonstrates that the target strength depends on the ellipsoid's geometric dimensions and the incident angle. This section examines the variations in ellipsoid target strength under different incident angles for non-proportional scaling:

1) incidence angle 0°:
when the incident angle $\varphi = 0°$, substituting into the equation $\tan v_0 = (b/a)\tan\varphi$, we obtain $v_0 = k\pi$. At this point, the target strength of the ellipsoid is

$$\mathrm{TS} = 10\log(H(\mathbf{r}\omega)) = 20\log\left(\frac{b^2}{2a}\right). \tag{13}$$

The major semi-axes of the ellipsoid, a and b, are scaled by the scaling factors N_x and N_y, respectively, such that $a = N_x a'$ and $b = N_y b'$, where the variables in the scaled model are denoted with a prime ($'$). The difference in target strength between the scaled model and the prototype is given by

$$\Delta\mathrm{TS} = \mathrm{TS} - \mathrm{TS}' = 20\log(N_y^2/N_x); \tag{14}$$

2) incidence angle 90°:
when the incident angle $\varphi = 90°$, substituting into the equation $\tan v_0 = (b/a)\tan\varphi$, we obtain $v_0 = \pi/2 + k\pi$. At this point, the target strength of the ellipsoid is

$$\mathrm{TS} = 10\log(H(\mathbf{r}\omega)) = 20\log\left(\frac{a}{2}\right). \tag{15}$$

The major semi-axes of the ellipsoid, a and b, are scaled by the scaling factors N_x and N_y, respectively, i.e., $a = N_x a'$ and $b = N_y b'$, where the variables in the scaled model are denoted with a prime ($'$). The difference in target strength between the scaled model and the prototype is

$$\Delta\mathrm{TS} = \mathrm{TS} - \mathrm{TS}' = 20\log(N_x). \tag{16}$$

For an ellipsoid with a major axis of 38 m and a minor axis of 2 m, the major axis is scaled down by a factor of 2, while the minor axis remains unchanged. The target strength is calculated for sound wave incident angles of 0° and 90°, considering both reception and transmission alignment. The target strength is then corrected using the derived method, and the corrected results are presented in Fig. 6.

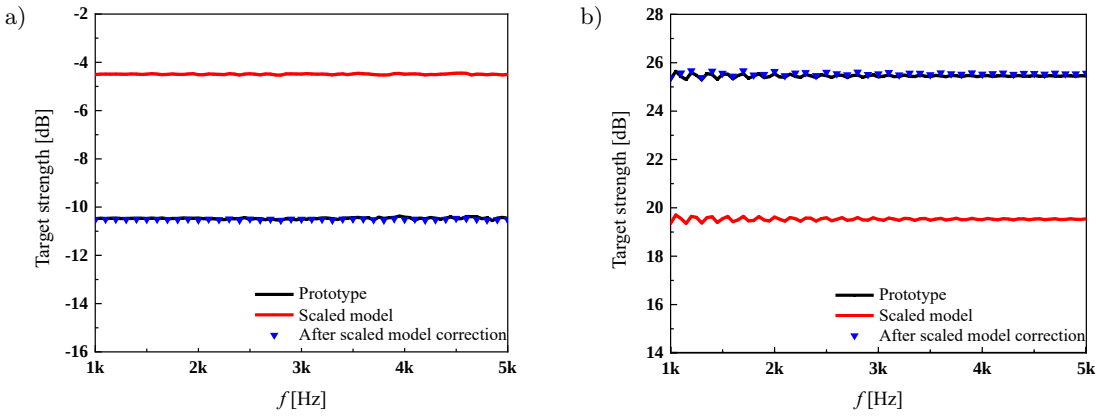

Fig. 6. Target strength of the ellipsoid with a non-isotropic scaling model after correction: a) incident angle of 0°, b) incident angle of 90°.

As shown in Fig. 6, with the reduction of the ellipsoid's major axis, the target strength correction for the scaled model at an incident angle of 0° is −6.02 dB. The corrected result is presented in Fig. 6a, and the average

absolute error between the corrected scaled model's target strength and the prototype's target strength is 0.05 dB. At an incident angle of 90°, the target strength correction for the scaled model is 6.02 dB. The correction result is shown in Fig. 6b, and the average absolute error between the corrected scaled model's target strength and the prototype's target strength is 0.10 dB.

3.2. Correction of target strength for a finite-length elliptical cylinder

According to the target strength equation for the finite-length elliptical cylinder derived in Subsec. 2.2, the target strength of the finite-length cylinder depends on the its geometric dimensions, incident angle, and incident frequency. This section examines the variation in target strength after non-isotropic scaling under different incident angles.

The variables a, b, and h are scaled by scale factors N_x, N_y, and N_z, respectively, i.e., $a = N_x a'$, $b = N_y b'$, $h = N_z h'$, where the relevant variables of the scaled model are denoted with primes ($'$). The difference in target strength between the scaled model and the prototype is expressed as

$$\Delta \mathrm{TS} = \mathrm{TS} - \mathrm{TS}' = 20\log(I\lambda'/I'\lambda). \tag{17}$$

From the above equation, it can be seen that the variation in target strength of the non-isotropically scaled model is related to the value of $I\lambda'/I'\lambda$. The he value of $I\lambda'/I'\lambda$ can be expressed as follows:

$$\frac{I\lambda'}{I'\lambda} = \left(\frac{f}{f'}\right)^{1/2} N_x N_y N_z \left(\frac{a'^2\cos^2\varphi + b'^2\sin^2\varphi}{(N_x a')^2\cos^2\varphi + (N_y b')^2\sin^2\varphi}\right)^{3/4}; \tag{18}$$

1) incidence angle is 0°:
when the incident angle is 0°, i.e., $\varphi = 0°$, the target strength formula can be simplified to:

$$\frac{I\lambda'}{I'\lambda} = \left(\frac{f}{f'}\right)^{1/2} \frac{N_y N_z}{\sqrt{N_x}}; \tag{19}$$

2) incidence angle is 90°:
when the incident angle is 90°, i.e., $\varphi = 90°$, the target strength formula can be simplified to:

$$\frac{I\lambda'}{I'\lambda} = \left(\frac{f}{f'}\right)^{1/2} \frac{N_x N_z}{\sqrt{N_y}}. \tag{20}$$

The target strength of an elliptical cylinder with a long semi-axis $a = 4$ m, a short semi-axis $b = 2$ m, and a height $h = 10$ m is calculated for frequencies ranging from 1 kHz to 10 kHz with a step size of 100 Hz. A scaled model 1 is constructed with a long semi-axis $a = 4$ m, a short semi-axis $b = 2$ m, and a height $h = 6$ m, and the target strength is calculated for the same frequency range and step size. A scaled model 2 is constructed with a long semi-axis $a = 2$ m, a short semi-axis $b = 1$ m, and a height $h = 10$ m, and the target strength is calculated again for the same frequency range and step size.

As shown in Fig. 7, as the height of the elliptical cylinder decreases, the corrected scaled-model target strength becomes 4.43 dB. The correction result is presented in Fig. 7a, where the corrected scaled model target strength closely matches the original target strength. As the semi-major and semi-minor axes of the elliptical base are scaled, the corrected scaled model target strength is 3.01 dB. The correction result is shown in Fig. 7b, where the corrected scaled model target strength closely matches the prototype target strength.

3.3. Correction of target strength for an elliptical frustum

According to the target strength formula for the truncated elliptical frustum derived in Subsec. 2.3, it is known that the target strength of the truncated elliptical frustum depends on the geometric dimensions, incident

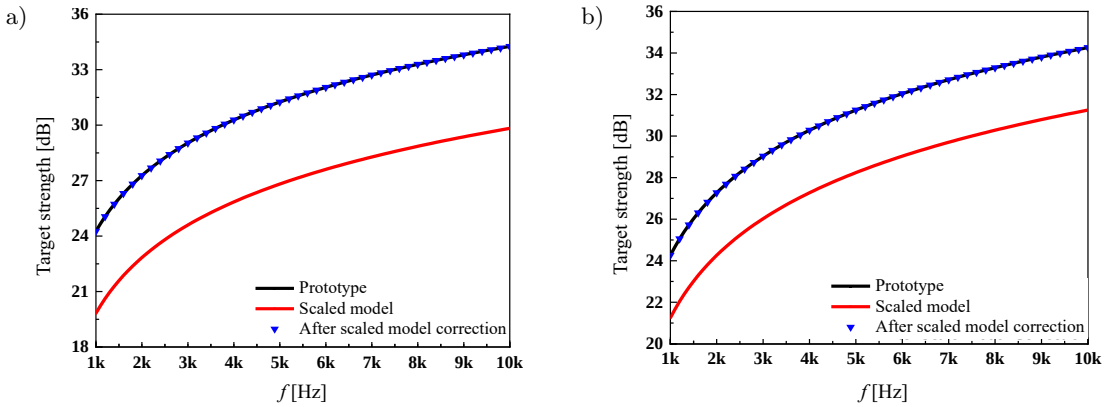

Fig. 7. Comparison of the original target strength and the corrected scaled-model target strength: a) model 1, b) model 2.

angle, and incident frequency. This section discusses the variation in the target strength of the truncated elliptical frustum after non-isotropic scaling, specifically for an incident angle of 90°.

When the incident angle is 90°, i.e., $\theta = 90°$, the target strength formula can be simplified as follows:

$$A_1 = \frac{1}{4}\sqrt{\frac{L}{\pi k}}\frac{\eta^{3/2}\tan^{1/2}\beta}{(\sin^2\varphi+\eta^2\cos^2\varphi)^{1/4}}\frac{(\sin^2\varphi+\eta^2\cos^2\varphi)^{-1/2}}{\tan\beta(\sin^2\varphi+\eta^2\cos^2\varphi)^{1/2}}, \tag{21}$$

$$A_2 = \frac{1}{4}\sqrt{\frac{L_1}{\pi k}}\frac{\eta^{3/2}\tan^{1/2}\beta}{(\sin^2\varphi+\eta^2\cos^2\varphi)^{1/4}}\frac{(\sin^2\varphi+\eta^2\cos^2\varphi)^{-1/2}}{\tan\beta(\sin^2\varphi+\eta^2\cos^2\varphi)^{1/2}}. \tag{22}$$

For the case of a circular base frustum ($\eta = 1$) and $\varphi = 0°$:

$$A_1 = \frac{1}{4}\sqrt{\frac{L}{\pi k}}\frac{1}{\tan^{1/2}\beta}, \qquad A_2 = \frac{1}{4}\sqrt{\frac{L_1}{\pi k}}\frac{1}{\tan^{1/2}\beta}.$$

From the aforementioned equations, it can be seen that the change in target strength of the non-geometrically scaled model is related to the half-apex angle β, and the value of β depends on the geometric dimensions of the truncated cone. Next, we discuss the relationship between the length scale ratio of the truncated cone and the half-apex angle β. The radius of the truncated cone base a and the height L are scaled by the scale factors N_x and N_y, respectively, i.e., $a = N_x a'$ and $L = N_y L'$, where the variables for the scaled model are denoted with a prime. The difference in target strength between the scaled model and the prototype is

$$\Delta\mathrm{TS} = \mathrm{TS} - \mathrm{TS}' = 20\log\left(\frac{A_1 + A_2}{A_1' + A_2'}\right), \tag{23}$$

$$\Delta\mathrm{TS} = 20\log\left(\frac{\tan^{1/2}\beta'}{\tan^{1/2}\beta}\frac{\sqrt{L}+\sqrt{L_1}}{\sqrt{L'}+\sqrt{L_1'}}\right). \tag{24}$$

As shown in Fig. 5, $\tan\beta = a/L$ and $\tan\beta' = a'/L'$. The relationship between the target strength difference and the scale ratio can thus be expressed as

$$\Delta\mathrm{TS} = 20\log\left(\frac{N_y}{\sqrt{N_x}}\right). \tag{25}$$

The target strength of a truncated cone with a lower base radius of 4 m, an upper base radius of 1 m, and a height of 6 m is calculated for frequencies ranging from 1 kHz to 10 kHz and a step size of 100 Hz. Scaled model 1 is constructed with a lower base radius of 2.4 m, an upper base radius of 0.6 m, and a height of 6 m, and its target strength is calculated over the same frequency range and step size. Scaled model 2 is constructed with a lower base radius of 4 m, an upper base radius of 1 m, and a height of 4 m, and its target strength is also calculated for the same frequency range and step size.

As shown in Fig. 8, with the scaling of the semi-major and semi-minor axes of the base ellipse, the correction value for the target strength of the scaled model is 2.21 dB, as illustrated in Fig. 8a. The corrected target strength of the scaled model closely matches that of the prototype. As the height of the elliptical cone is reduced, the correction value for the target strength of the scaled model increases to 3.01 dB, with the corrected result shown in Fig. 8b. The average absolute error between the corrected target strength of the scaled model and the prototype target strength is 0.24 dB.

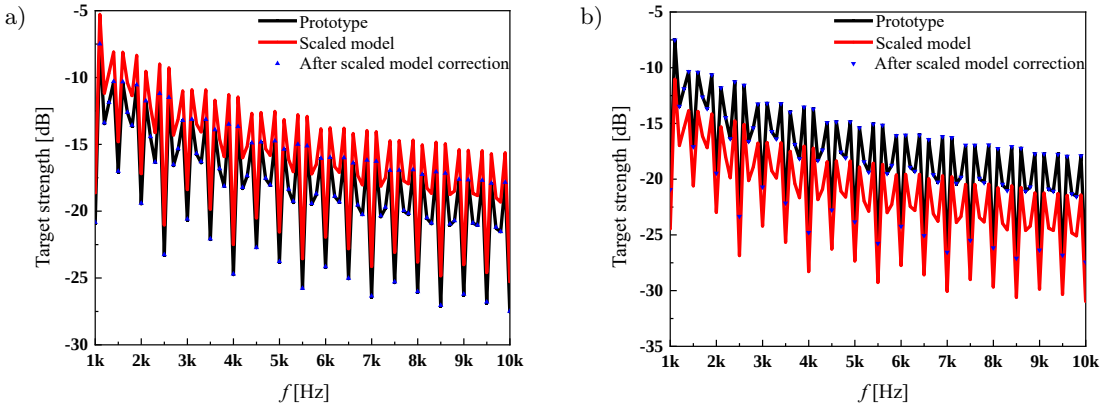

Fig. 8. Comparison of the original target strength and the corrected scaled-model target strength: a) model 1, b) model 2.

4. Target strength correction of the non-geometrically scaled model for the combined structure

A typical underwater vehicle is composed of simple geometric components such as ellipsoids, cylinders, and truncated elliptical frustum. Using the method of energy superposition, the target strength of the combined structure is given by

$$\mathrm{TS} = 10\log\left(10^{\left(\frac{\mathrm{TS}_1}{10}\right)} + 10^{\left(\frac{\mathrm{TS}_2}{10}\right)} + 10^{\left(\frac{\mathrm{TS}_3}{10}\right)}\right), \tag{26}$$

where TS represents the target strength of the combined structure, and TS_1 to TS_3 represent the target strengths of the individual geometric components. After the combined structure undergoes non-geometrical scaling, the target strengths of each component are denoted as TS', TS'_1 to TS'_3. At this point, each component has a corresponding correction factor $\Delta\mathrm{TS}_1$ to $\Delta\mathrm{TS}_3$, and the following equation holds:

$$\mathrm{TS} = 10\log\left(10^{\left(\frac{\mathrm{TS}'_1+\Delta\mathrm{TS}_1}{10}\right)} + 10^{\left(\frac{\mathrm{TS}'_2+\Delta\mathrm{TS}_2}{10}\right)} + 10^{\left(\frac{\mathrm{TS}'_3+\Delta\mathrm{TS}_3}{10}\right)}\right). \tag{27}$$

If the correction values for each component are the same ($\Delta\mathrm{TS}_1 = \Delta\mathrm{TS}_2 = \Delta\mathrm{TS}_3 = \Delta\mathrm{TS}$), the formula can be simplified to:

$$\mathrm{TS} = \mathrm{TS}' + \Delta\mathrm{TS}. \tag{28}$$

This study designs a rotational body model composed of an ellipsoid, a cylinder, and a conical frustum. In practical applications, the correction methods for different regions of a complex model are not identical, and the actual correction coefficients for each region can vary. In such cases, the scaling model correction coefficients must be solved separately for each region to complete the target strength correction. The method proposed in this paper uses the geometric highlight model formula, applying non-proportional scaling to the geometric- dimension-related variables in the formula to determine the difference between the target strength of the non-geometrically scaled model and that of the prototype. This enables rapid correction of the scaled model's target strength for practical engineering applications.

The model consists of a head ellipsoid, a central cylinder, and a tail concentric frustum. The interior of the complex model is filled with air, and the specific parameters of the model are shown in Fig. 9, where L_1 is the long radius of the model's shell ellipsoid (5 m), L_2 is the length of the model's shell cylinder (10 m), L_3 is the

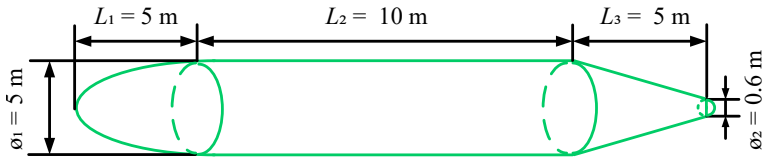

Fig. 9. Schematic diagram of the complex model dimensions.

height of the model's shell frustum (5 m), $\varnothing_1$ is the diameter of the model's shell cylinder (5 m), and $\varnothing_2$ is the diameter of the small end face of the model's shell frustum (0.6 m).

To calculate the target strength of the complex model, the calculation frequency ranges from 1 kHz to 10 kHz with a step size of 100 Hz. For length-scaled model 1 (Fig. 10a): the length of the complex model is scaled down by a factor of 0.75, while the radius of the rotational body remains unchanged. The calculation frequency is 1 kHz to 10 kHz with a step size of 100 Hz. For radius-scaled model 2 (Fig. 10b): the radius of the complex model is scaled down by a factor of 0.6, while the length of the rotational body remains unchanged. The calculation frequency is 1 kHz to 10 kHz with a step size of 100 Hz.

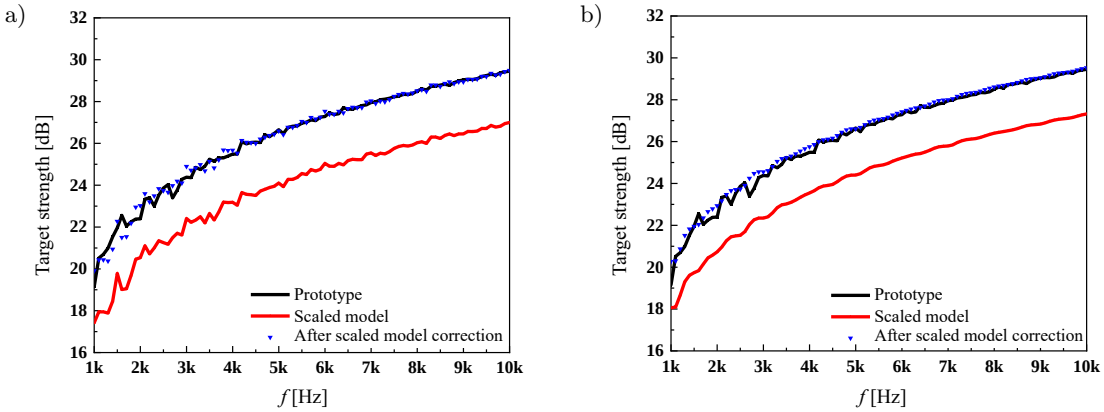

Fig. 10. Comparison of the original target strength and the corrected scaled model target strength: a) length-scaled model 1, b) radius-scaled model 2.

As shown in Fig. 10, as the height of the ellipsoid cylinder decreases, the target strength correction of the scaled model is 2.49 dB. The correction results are shown in Fig. 10a, where the average absolute error between the corrected scaled model's target strength and the prototype's target strength is 0.16 dB. As the semi-major and semi-minor axes of the bottom ellipse are scaled, the target strength correction of the scaled model is 2.21 dB. The correction results are shown in Fig. 10b, where the average absolute error between the corrected scaled model's target strength and the prototype's target strength is 0.18 dB.

5. Conclusions

This paper investigated simple targets (ellipsoids, finite-length cylinders, and frustums of elliptical cones) as well as rotating bodies. Based on the highlight model theory, the paper analyzed the impact of geometric size changes in scaled models on target strength and established a correction formula for non-proportionally scaled models. The feasibility of this target strength correction method was verified using plate element methods. The main conclusions are as follows:

1. This paper proposes a correction method suitable for the mid-to-high frequency range. The method, based on the highlight model theory, addresses geometric scales in the target strength solution formula by considering proportional changes in the geometric scales. It summarizes the target strength variation law and develops a corresponding correction method. However, the omission of low-frequency elastic resonance reduces the accuracy of the target strength correction. Additionally, geometric target strength is closely related to

the angle of incidence of the sound waves. This paper also discusses the target strength correction method for non-proportional scaled models under specific incident-angle conditions.

2. Non-proportional scaled models of simple geometric targets (ellipsoids, cylinders, and frustums of cones) can be corrected using the highlight model theory. When correcting the target strength of an ellipsoid non-proportional scaled model, the scale ratio of the semi-major and semi-minor axes must be considered. For a finite-length cylinder, the scale ratios of the cylinder's base radius and height are important. For a frustum of a cone, the scale ratios of the cone's height and base radius need to be accounted for. After correction, the target strength of these simple geometric models is generally consistent with that of the prototype.
3. The rotating body model designed in this paper consists of an ellipsoid, a cylinder, and a frustum of a cone. For the non-proportional scaled model of this combined body, the paper, based on the highlight model theory and using the energy superposition method, derives the target strength correction method. The complex model exhibits significant curvature changes at the junction of the cylinder and the frustum of the cone. When sound waves are incident at this junction, corner waves are generated. In this case, the correction method based on the energy superposition method introduces some errors.
4. The correction method proposed in this paper is designed for rapid target strength correction of scaled models under engineering-scale characteristic-angle conditions, utilizing the highlight model theory. In practical applications, the scale ratios of different parts of the same model can vary. As the incident angle changes, the model's target strength solution formula also changes. Therefore, different incident angles must be considered separately, as the target strength value varies with the incident angle, and the correction coefficient cannot be represented by a single numerical value. When correcting the target strength of complex models, it is essential to analyze the incident-reflection conditions of different components and account for the impact of various incident angles. Different components require different correction coefficients.

Currently, correction methods for scaled models are mainly applied to shell vibration and acoustic radiation similarity, while research on sound-scattering similarity correction methods is relatively limited. This paper proposes a rapid target strength correction method for scaled models in engineering applications, achieving certain correction effects. However, the accuracy and applicability of this method still require further improvement.

Fundings

This work was supported by the National Natural Science Foundation of China (grant no. 52201397) and the Open Fund of the National Key Laboratory of Ship Vibration and Noise (grant no. 6142204230709 and no. 6142204240202).

Conflict of interest

The authors declare that they have no known competing financial interests or personal relationships that could have appeared to influence the work reported in this paper.

Authors' contributions

Jin Zhang conceptualized the study and wrote the original draft. Zhenyu Li performed the analysis and contributed to data interpretation. Yinhao Li and Zilong Peng performed the analysis and wrote the original draft. All authors reviewed and approved the final manuscript.

References

1. Agounad S., Décultot D., Chati F., Léon F., Khandouch Y. (2023), Experimental study of the bistatic acoustic scattering from cylindrical shell, *Mechanical Systems and Signal Processing*, **186**: 109892, https://doi.org/10.1016/j.ymssp.2022.109892.

2. Agounad S., Décultot D., Chati F., Leon F., Khandouch Y., Elhanaoui A. (2020), Acoustic scattering from cylindrical shell: Monostatic versus bistatic configurations [in French], *Forum Acusticum*, pp. 1863–1866, https://doi.org/10.48465/fa.2020.0610.

3. Fan J., Tang W.L., Zhou L.K. (2012), Planar elements method for forecasting the echo characteristics from sonar targets [in Chinese], *Journal of Ship Mechanics*, **16**(Z1): 171–180, https://doi.org/10.3969/j.issn.1007-7294.2012.01.020.

4. Feng M. *et al.* (2025), A TDOA sequence estimation method of underwater sound source based on hidden Markov model, *Applied Acoustics*, **227**: 110238, https://doi.org/10.1016/j.apacoust.2024.110238.

5. Gao T., Lin Y. (2019), Model analysis, design and experiment of a fan-wing underwater vehicle, *Ocean Engineering*, **187**: 106101, https://doi.org/10.1016/j.oceaneng.2019.06.006.

6. Ge J., Luo T., Qiu J. (2024), Discretized macro-element method to evaluate the crushing behavior and protective performance of crashworthy devices under ship collisions, *Ocean Engineering*, **306**: 118125, https://doi.org/10.1016/j.oceaneng.2024.118125.

7. Huijgens L., Vrijdag A., Hopman H. (2021), Hardware in the loop experiments with ship propulsion systems in the towing tank: Scale effects, corrections and demonstration, *Ocean Engineering*, **226**: 108789, https://doi.org/10.1016/j.oceaneng.2021.108789.

8. Ke H., Peng Z., Zhou F., Chen T. (2024), Prediction method and characteristics of static acoustic scattering from marine propellers [in Chinese], *Acta Armamentarii*, **45**(5): 1523–1533, https://doi.org/10.12382/bgxb.2023.0017.

9. Li C., Wang D., Liu J. (2020), Numerical analysis and experimental study on the scaled model of a container ship lashing bridge, *Ocean Engineering*, **201**: 107095, https://doi.org/10.1016/j.oceaneng.2020.107095.

10. Liu J., Peng Z., Fan J., Liu Y., Kong Z. (2023), Research on the acoustic scattering prediction methodology of underwater vehicle based on sliced-parameterized multi-highlights model [in Chinese], *Acta Armamentarii*, **44**(2): 517–525, https://doi.org/10.12382/bgxb.2021.0764.

11. Liu Y., Pi A., Yang H., Feng J., Huang F. (2020), Study on similarity law of non-proportionally scaled penetration/perforation test [in Chinese], *Explosion and Shock Waves*, **40**(03): 033302, https://doi.org/10.11883/bzycj-2019-0086.

12. Liu Z., Shi X., Guo T., Ren H., Zhang M. (2024), Investigation on hydrodynamic response and characteristics of a submerged floating tunnel based on hydrodynamic tests, *Ocean Engineering*, **300**: 117187, https://doi.org/10.1016/j.oceaneng.2024.117187.

13. Liu Z.X., Song Y., Yang Q.X. (2017), Research on foreign free maneuvering submarine models experiment [in Chinese], *Ship Science and Technology*, **39**(17): 194–199.

14. Schneider H.G. *et al.* (2003), Acoustic scattering by a submarine: Results from a benchmark target strength simulation workshop, [in:] *Tenth International Congress on Sound and Vibration.*

15. Stulenkov V.A. *et al.* (2024), Physical modeling of the hydroacoustic field of a marine propeller, *Acoustical Physics*, **70**(5): 872–879, https://doi.org/10.1134/s1063771024601912.

16. Tang W.L. (1994), Highlight model of echoes from sonar targets, *ACTA Acustica*, **19**(2): 92–100, https://doi.org/10.15949/j.cnki.0217-9776.1994.02.004.

17. Tang W.L., Fan J., Ma Z.C., Ji S. (2018), Acoustic scattering of underwater targets [in Chinese], *Beijing*: *Science Press*, https://doi.org/10.15949/j.cnki.0371-0025.2018.05.020.

18. Tao W., Liu Y., Long R., Cheng L. (2025), A time series CGAN denoising model targeting vessel's radiated noise for underwater acoustic communications, *Ocean Engineering*, **318**: 120076, https://doi.org/10.1016/j.oceaneng.2024.120076.

19. Ting Z., Yang T.C., Wen X. (2019), Bistatic localization of objects in very shallow water, *IEEE Access*, **7**: 180640–180651, https://doi.org/10.1109/ACCESS.2019.2947851.

20. Wang S., Xu F., Zhang X., Yang L., Liu X. (2021), Material similarity of scaled models, *International Journal of Impact Engineering*, **156**: 103951, https://doi.org/10.1016/j.ijimpeng.2021.103951.

21. Wang Y., Wang Q., Wang D. (2023), Scaling characteristics of the unified similarity criterion for geometrically distorted scale models, [in:] *ASME 2023 42nd International Conference on Ocean, Offshore and Arctic Engineering*, https://doi.org/10.1115/OMAE2023-101312.

22. Wang Y., Wei P., Wang Q., Dai Z., Wang D. (2024), A new similarity method for the ultimate strength of box girders subjected to the combined load of bending and lateral pressure, *Ocean Engineering*, **313**(Part 1): 119270, https://doi.org/10.1016/j.oceaneng.2024.119270.

23. Xue Y., Peng Z., Yu Q., Zhang C., Zhou F., Liu J. (2023), Analysis of acoustic scattering characteristics of underwater targets based on Kirchhoff approximation and curved triangular mesh [in Chinese], *Acta Armamentarii*, **44**(8): 2424–2431, https://doi.org/10.12382/bgxb.2022.0374.

24. Yan T., Wang K. (2025), Application and control mechanism of thin film metamaterials in underwater sound-absorbing materials at low frequency under high hydrostatic pressure, *Applied Acoustics*, **231**: 110535, https://doi.org/10.1016/j.apacoust.2025.110535.

25. Yu M., Lu S. (2001), Investigation of acoustic scale effects for large size model of submarine compartment [in Chinese], *Journal of Ship Mechanics*, **5**(5): 50–55, https://doi.org/10.3969/j.issn.1007-7294.2001.05.007.

26. Yu M., Shi X., Chen K. (1999), Study on acoustic similitude of elastic stiffened cylindrical shells by FEM and BEM [in Chinese], *Shipbuilding of China*, **1999**(3): 65–71.

27. Yu M., Wang Z., Lu S. (2002a), Analysis of acoustic similarity of mechanical system for underwater vehicle by energy method [in Chinese], *Journal of Ship Mechanics*, **6**(4): 96–102, https://doi.org/10.3969/j.issn.1007-7294.2002.04.011.

28. Yu M., Wu Y., Lu S. (2002b), Experiment investigation on acoustic similarity of stiffened cylindrical shells [in Chinese], *Shipbuilding of China*, **43**(2): 52–59, https://doi.org/10.3969/j.issn.1000-4882.2002.02.008.

29. Zhang L., Yang D. (2001), Similarity of sound field of shell radiation with dissimilar item [in Chinese], *Journal of Harbin Engineering University*, **22**(3): 30–32, https://doi.org/10.3969/j.issn.1006-7043.2001.03.008.

30. Zhou L., Xiong C., Duan Y., Wu J., Sun Y., Wei Q. (2021), Design of a dynamic scaled model for marine propulsion shafting [in Chinese], *Journal of Ship Mechanics*, **25**(7): 973–980, https://doi.org/10.3969/j.issn.1007-7294.2021.07.015.